2015

Fast strain wave induced magnetization changes in long cobalt bars: Domain motion versus coherent rotation

S Davis
University of Nebraska-Lincoln

J A. Borchers
National Institute of Standards and Technology

B B. Maranville
National Institute of Standards and Technology

Shireen Adenwalla
University of Nebraska-Lincoln, sadenwalla1@unl.edu

Fast strain wave induced magnetization changes in long cobalt bars: Domain motion versus coherent rotation

S. Davis,[1,a)] J. A. Borchers,[2] B. B. Maranville,[2] and S. Adenwalla[1,b)]
[1]*Department of Physics and Astronomy and Nebraska Center for Materials and Nanoscience, University of Nebraska-Lincoln, Lincoln, Nebraska 68588-0299, USA*
[2]*NIST Center for Neutron Research, National Institute of Standards and Technology, Gaithersburg, Maryland 20899, USA*

(Received 8 December 2014; accepted 25 January 2015; published online 11 February 2015)

A high frequency (88 MHz) traveling strain wave on a piezoelectric substrate is shown to change the magnetization direction in 40 μm wide Co bars with an aspect ratio of 10^3. The rapidly alternating strain wave rotates the magnetization away from the long axis into the short axis direction, via magnetoelastic coupling. Strain-induced magnetization changes have previously been demonstrated in ferroelectric/ferromagnetic heterostructures, with excellent fidelity between the ferromagnet and the ferroelectric domains, but these experiments were limited to essentially dc frequencies. Both magneto-optical Kerr effect and polarized neutron reflectivity confirm that the traveling strain wave does rotate the magnetization away from the long axis direction and both yield quantitatively similar values for the rotated magnetization. An investigation of the behavior of short axis magnetization with increasing strain wave amplitude on a series of samples with variable edge roughness suggests that the magnetization reorientation that is seen proceeds solely via coherent rotation. Polarized neutron reflectivity data provide direct experimental evidence for this model. This is consistent with expectations that domain wall motion cannot track the rapidly varying strain. © *2015 AIP Publishing LLC*. [http://dx.doi.org/10.1063/1.4907580]

I. INTRODUCTION

The fastest times for magnetization reversal in nanoscale ferromagnets are limited by the time scales for angular momentum and energy exchange.[1,2] Experiments using fast light pulses,[3] short magnetic field pulses,[4] and heat as the initial trigger have established that the fastest reversal of magnetization occurs over time scales of the order of 100 ps. The mode of excitation and the properties of the ferromagnet (the saturation magnetization, the shape, and magneto-crystalline anisotropies) dictate the fastest switching times for a particular system.[1,2]

Strain has been shown to be an attractive and successful route to control of magnetization, albeit on slow (dc) time scales. The canonical heterostructure of ferroelectric (FE) $BaTiO_3$ and ferromagnetic (FM) CoFe shows almost perfect domain pattern transfer between the FE and FM. Electric field induced changes in the underlying FE domains result in imprinting of the FM domains,[5] due to the elastic coupling between the FE and FM. The resulting strains within the FM material alter the magnetic anisotropy axes (as confirmed by element specific x-ray scattering experiments[6]) and hence the domain patterns.

Our experiments extend strain-induced magnetization control to short (~10 ns) timescales, using high frequency surface acoustic waves to produce a periodic strain wave. Excitation of the magnetization via phonons (as compared to photons) has often been restricted to heat pulses, which necessarily involve a wide range of frequencies with a spectral distribution that is difficult to control. In contrast, surface acoustic wave (SAW) driven phonon excitation is controlled for both frequency and amplitude using high frequency, monochromatic strain waves that exploit the coupling between strain and magnetization to trigger changes in the direction of magnetization. Earlier experiments investigating the interactions of SAW with ferromagnetic thin films[7–10] measured changes in the SAW propagation amplitude resulting from changes in the magnetization direction. A recent more sophisticated analysis of the changes in the transmitted SAW amplitude and phase[11,12] across a Ni thin film indicates that the SAW excites ferromagnetic resonance (FMR) modes in the film. Ultra-short pulsed longitudinal acoustic excitations[13] triggered in glass substrates via femtosecond laser pulses, have been shown to result in rapid precession of the magnetization of a thin Ni film on the glass substrate, driven by the short strain pulse in the glass.

Our experiments at a driving SAW frequency of 88 MHz differ from previous SAW driven magnetization experiments in two ways. First, our experiments[14] *directly* measure the magnetization rotation of a lithographically defined array of 10 nm thick rectangular Co bars (10 μm × 40 μm) from the long axis into the short axis direction. Moreover, in these experiments, the SAW frequency of 88 MHz is well below the calculated precession frequency (>2 GHz), the damping times (~1 ns) of the bars are well below the time period of 11 ns, and hence we assume that the magnetization switches instantaneously on the time scale of the SAW wave. Fast SAWs, with frequencies on the order of

[a)]Presently at Department of Physics, Northwestern University, Evanston, Illinois 60208, USA.
[b)]Author to whom correspondence should be addressed. Electronic mail: sadenwalla1@unl.edu

100 MHz, provide sufficient strain to overcome the shape anisotropy, and the magnetization switches between the long and short axes at the frequency of the SAW. These experiments[14] indicate that there exists a threshold strain below which the magnetization does not rotate and that this threshold strain depends on external magnetic field and exchange bias in a manner that is consistent with a free energy model that assumes coherent rotation of the magnetization. In addition, measurements with increasing and decreasing strain indicate no hysteresis, consistent with the coherent rotation model. From these preliminary experiments, we conclude that SAW present a novel and realistic route for the investigation of fast magnetization dynamics, because SAW at the frequency of interest (~10 GHz) are readily available.

II. EXPERIMENTAL METHODS

A. Sample growth

Each sample consists of a pair of interdigitated transducers (IDTs) on Z cut $LiNbO_3$ wafers. The IDTs are 2 cm long, with 10 μm wide fingers, spaced 10 μm apart, resulting in a 40 μm wavelength for the propagating wave (see Figure 1(a)). The IDT pattern is repeated 100 times to ensure a sharp resonance and sizeable strain wave amplitude. The propagation axis of the resulting SAW is the crystalline y-axis of the $LiNbO_3$, resulting in a resonance frequency of 88.2 MHz and a quality factor $Q = f_0/\Delta f = 136$, where f_0 and Δf are the resonance frequency and the FWHM of the resonance, respectively. An array of 30 nm thick Co bars 12 μm wide, 2 cm long and spaced at 20 μm (at half the wavelength of the SAW), is patterned between the two IDTs, resulting in a fractional Co coverage of 1/1.65, as confirmed by atomic force microscopy (AFM) measurements (Figure 2). Both the IDT's and the bars are patterned using photolithography and magnetron sputter deposition. The sample set consisted of five samples that differed only in the edge roughness of the Co bars, a roughness that is controlled by systematic under/over development of the photolithographic patterns. The edge roughness is obtained from AFM measurements of the Co bars, using Gwyddion a free modular software package available for SPM analysis (http://gwyddion.net). We fit a straight line to the edge and obtain the rms deviation from this straight line, resulting in edge roughnesses ranging from 1.8 nm to 7.4 nm. The sample used for the PNR measurements has an rms edge roughness of 2.3 nm.

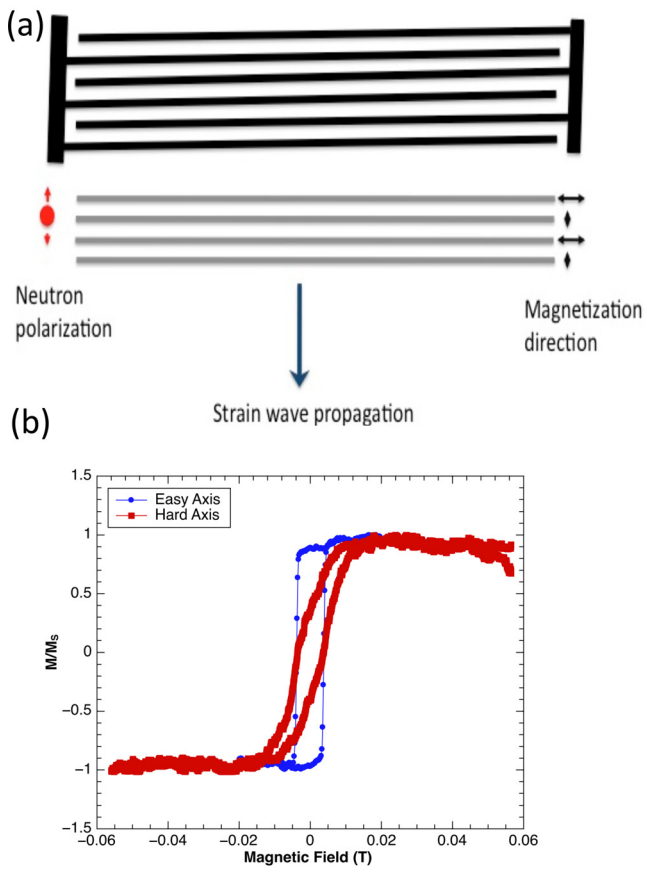

FIG. 1. (a) Geometry of the SAW transducer and the magnetic bars. The spatial periodicity of the bars is $\lambda/2$ and the arrows indicate the magnetization direction at a particular instant of time when the SAW is driven at the resonant frequency. For the PNR measurements, the sample was oriented with the neutron polarization direction parallel to the short axis of the bars and the scattering vector perpendicular to the film plane. (b) Easy and hard axes MOKE hysteresis loops of the sample used for PNR, with an edge roughness of 2.3 nm.

B. Polarized neutron reflectivity

Polarized neutron reflectivity (PNR) allows for the determination of the absolute magnetization along and perpendicular to the neutron spin polarization direction with excellent sensitivity as a function of depth.[28] In the present experiment, it quantifies the extent to which domain pinning and/or coherent rotation dominates the strain-driven reorientation process. PNR measurements were performed at the NIST Center for Neutron Research on the NG1 and AND/R reflectometers to fully characterize the uniformity of the Co

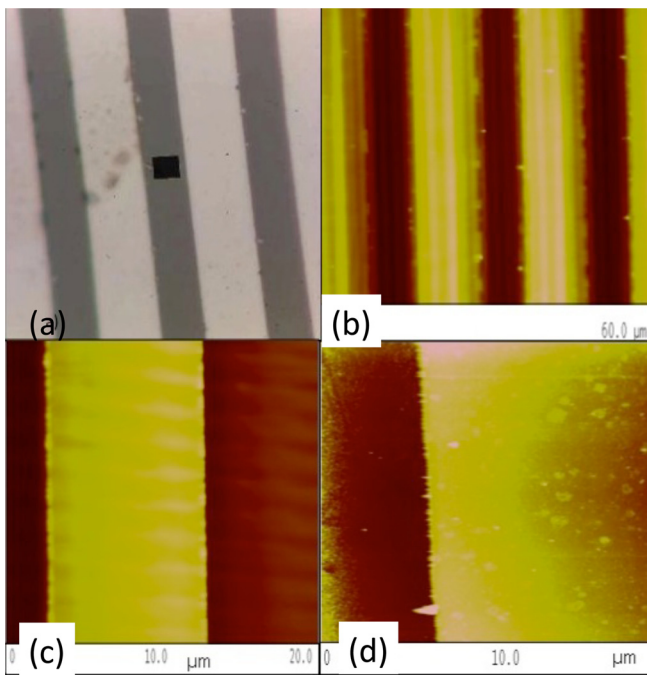

FIG. 2. Optical (a) and AFM (b)–(d) images of the 12 μm wide Co bars in successive samples with increasing roughness.

magnetization during the switching process. In general, PNR is sensitive to the nanoscale depth-dependence of the vector magnetization, as well as to the chemical composition, averaged across the sample plane. The magnetization extracted from the PNR data is quantitative and does not require normalization by sample mass or volume, in contrast to magneto optical Kerr effect (MOKE). In addition, the neutron reflectivity is not dependent upon changes in the optical refractive index of the electro-optically active $LiNbO_3$. For these measurements, incident and scattered neutrons with wavelength of 0.475 nm (or 0.5 nm) were polarized parallel to the guide field using Fe-Si supermirrors, as described elsewhere.[29] Using Al-coil flippers before and after the sample, all four polarization cross sections were measured for each sample condition. The two non-spin flip (NSF) cross sections, R^{++} and R^{--}, are sensitive to the nuclear composition, and their difference is related to the projection of the magnetization parallel to the field (0.001 T or 0.1 T). The spin-flip (SF) cross sections, R^{+-} and R^{-+}, are sensitive only to the projection of the magnetization that is perpendicular to the applied guide field. (Note that the experimental configuration is shown schematically in Figure 1.) To enable straightforward data interpretation, the sample was oriented with the long stripes parallel to the beam direction. The scattering from the bare $LiNbO_3$ substrate and the Co stripes average incoherently in this configuration since the resolution perpendicular to the scattering plane is broad. The raw data were corrected[29] for instrumental effects including polarization efficiency (>97%), background, and beam footprint. The reduced data were then fit to models based on the Parratt formalism using REFL1D[26] reflectivity software in order to extract depth-dependent profiles for the nuclear scattering length density and vector magnetization.

C. Magneto optical Kerr effect measurements

The MOKE technique has been extensively discussed[30] and has distinct advantages in the measurements of thin ferromagnetic films, among them high sensitivity and the ability to measure a particular component of magnetization. MOKE measurements are obtained with a setup similar to that in Ref. 30 using a photo-elastic modulator (PEM) and a fast photodiode. The photodetector signal is fed to a lock-in operating at the frequency of the PEM. We measure only the time-averaged component of the magnetization[16] rather than the fast magnetization component at the resonant frequency, for reasons that are briefly discussed below. (A more extensive discussion may be found in Ref. 14.) All the MOKE data shown here were obtained with a 3 s time constant but data obtained at different time constants show similar behavior albeit with increased scatter.

Because MOKE measures only relative changes in magnetization, it is necessary to normalize every data set to the saturation magnetization of the sample so as to obtain *quantitative* information on magnetization changes with applied strain. Before each run, the sample is saturated along the long, easy axis of the bars at a field of 0.2 T, well above the saturation field observed in easy axis MOKE loops (see Figure 1). After the field is turned off, the samples are rotated by 90° so that the short axis is parallel with both the MOKE scattering plane and the field direction. This alignment is facilitated by the diffraction pattern obtained from light scattering off this periodic structure. The squareness of the long easy axis hysteresis loop ($M_R/M_S > 0.9$) ensures that the magnetization remains saturated along the long axis direction, an assumption that is confirmed by PNR measurements. In this orientation, the MOKE is sensitive only to the magnetization component along the short axis direction. The MOKE signal is measured on a lock-in amplifier as a function of increasing and decreasing voltage applied to the interdigital transducers at the resonance frequency of 88.2 MHz.

III. RESULTS AND DISCUSSION

The present work is motivated by the desire to investigate the limits of the coherent rotation model and to investigate the strain-driven formation of domains. As the aspect ratios and associated shape anisotropy of the Co structures increase, the threshold strain for coherent rotation of magnetization will increase, as will the likelihood of rotation within isolated domains. The latter is dependent on both the increased shape anisotropy, which makes coherent rotation into the short axis direction energetically less favorable, as well as on the increasing number of defects that result during the photolithographic production of longer bars that may provide nucleation sites for domain formation. A schematic of the samples is shown in Figure 1(a) indicating the SAW transducer, the long Co bars (10 μm × 25 mm) and the relative orientation of the strain and the neutron spin direction. Because it is difficult to quantify and control the presence or absence of nucleation and pinning sites, we fabricated a set of samples, each with Co bars of identical dimensions that differ only in the edge roughness, thereby providing an external "knob" with which to dial up the density of such sites. An optical microscopy image and AFM images are shown in Figure 2, clearly showing the increasing edge roughness.

Our data indicate that even in these long samples, where domain formation must play a significant role, coherent rotation is the major contributor to magnetization reorientation at these high frequencies. Specifically, the fast SAW waves drive a substantial fraction of the bars into the short axis direction via coherent rotation, but increasing edge roughness results in an increasing fraction of the sample being pinned along the long axis direction, impervious to rotation via fast SAW generated magnetostriction.

We report on measurements of the SAW triggered magnetization rotation using both PNR and MOKE. MOKE hysteresis loops along the long axis and short axis for one of the samples (the sample on which PNR measurements were performed at NIST) are shown in Figure 1(b). From the slope of the hard axis loop, we obtain a shape anisotropy of 2.17×10^3 J/m^3, which is comparable to the calculated value of 1.95×10^3 J/m^3 for these high aspect ratio Co rectangles.

Although our data indicate otherwise, we start with a simple coherent rotation model in order to obtain insight into the process of strain driven reorientation. The free energy of the Co bars may be written as

$$E = -\mu_0 M_S \mathrm{H}\cos\theta - K_S \cos^2(\theta) + B_1 e_{33} \sin^2(\theta), \quad (1)$$

where the three terms are the Zeeman energy, the shape anisotropy energy, and the strain energy, respectively. The strain energy is the product of B_1, the magneto-elastic coefficient for Co, and the strain, e_{33}, along the short y-axis and θ is the angle between the magnetization vector and long axis. In this convention, a negative value of $B_1 e_{33}$ lowers the energy along the short axis direction. Since B_1 for bulk Co is positive ($6 \times 10^6 \mathrm{N/m^2}$), only *compressive* strain will lead to rotation of the magnetization. Minimization of the free energy with respect to θ leads to the minimum compressive strain at which the magnetization will move away from the long axis direction, given by

$$|e_{33}| > \left[\frac{\mu_0 M_s H + 2K_s}{2B_1}\right]. \quad (2)$$

Because $LiNbO_3$ is electro-optically active with a large electro-optical coefficient,[14,15] detection at the excitation frequency will result in changes in the MOKE signal that are independent of the magnetization. DC MOKE, averaged over multiple cycles, eliminates this effect, because the electro-optic effect is linear with electric field.[15] In zero field, only two stable states exist with M pointing either along the long or short axis direction. Hence, in the coherent rotation model, the time dependent magnetization response of a *single* Co element to a sinusoidal driven IDT will be a square wave, with the magnetization pointing along the short axis direction once the threshold strain is reached and remaining in that direction for a time Δt, until the strain drops to below the threshold value. For a single Co element, the net dc component[16] of M along the short axis direction corresponds to the average signal $M_s \Delta t/T$, where M_s is the saturation magnetization, Δt is the time interval over which the magnetization remains along the short axis and T is the period of the strain excitation

The array of Co bars are alternately stretched and compressed along the short axis upon application of the SAW. Because they are spaced at $\lambda/2$, with *sufficient* applied compressive strain, we expect the magnetization of every other bar to be rotated along the short axis direction, with the remaining bars magnetized along the long easy axis, resulting in the magnetization pattern indicated in Figure 3.

The maximum dc MOKE signal we will measure in the limit of very large strain wave amplitude is related to the time integral of the magnetization as the strain wave propagates. In this limit, the threshold strain is much less than the strain wave amplitude, resulting in magnetization rotation at very small fractional amplitude of the strain wave. We consider two cases, one in which the bars act as single domain particles (as was the case in Ref. 14) and another in which the bar is large enough to break up into multiple domains, a more likely scenario for the long bars of the present sample. In the single domain case, the bars will switch into the short axis direction if the *net* strain integrated over the width of a single bar is compressive and above the threshold strain. At large strain amplitude, every other bar will be magnetized along the short axis for a *half* cycle of the strain wave. Over the next half cycle, the alternate set of bars is magnetized along the short axis direction. Averaged over the time period of the strain excitation, this will result in a net magnetization of Ms/2 along the short axis direction. If, however, the bar is larger than a single domain, magnetization rotation will only occur if *every* portion of the bar is subject to compressive strain above the threshold value. For large strain amplitudes, every other bar will be magnetized along the short axis direction for a *quarter* cycle of the strain wave. We illustrate this in Figure 3 where the magnetization direction of the bars as a function of time is shown for one period of the strain wave. Between $t = T/4$ and $t = T/2$ (where T is the period of the wave), the magnetization of the 1st, 3rd, and 5th bars rotate towards the short axis direction. The alternate set of bars (2nd and 4th) rotate into the short axis direction between $t = 3T/4$ and $t = T$. In the intervening time (i.e., for $0 < t < T/4$ and $T/2 < t < 3T/4$), the bars may be fully magnetized along the long axis, resulting in a net dc short axis magnetization of $M_S/4$ *or* local strain may drive individual domains into the short axis direction resulting in a net dc magnetization $> M_S/4$. In this scenario, the maximum dc magnetization measured can only be $< M_S/4$ if regions within the Co remain pinned along the long axis direction, impervious to rotation via magnetostriction.

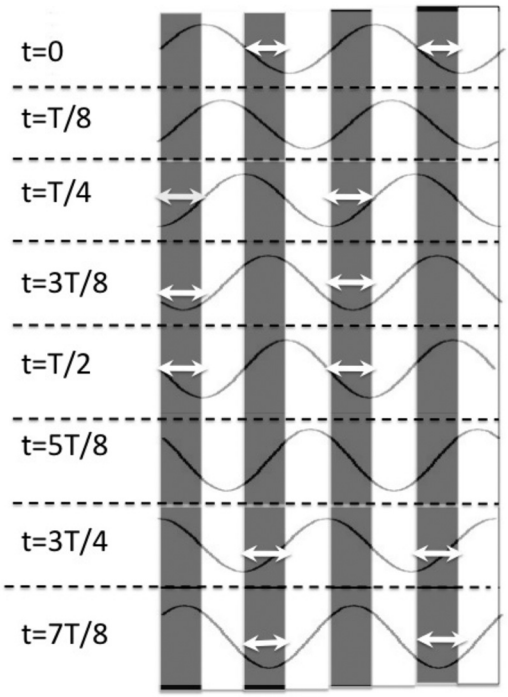

FIG. 3. Strain wave and the resulting magnetization rotation as a function of position and time. White arrows indicate the rotation of magnetization into the short axis direction. The time integral of the short axis magnetization for the scenario shown above will be $M_S/4$, where M_S is the saturation magnetization of the array.

Hence, the characteristic signature of dc MOKE measurements of the array along the short axis direction as a function of driving voltage are (i) a threshold voltage, $e_0 = e_1$, below which there is no component of magnetization along the in-plane short axis direction, followed by (ii) a subsequent increase in the dc MOKE signal with increased driving voltage, resulting from the increase in $\Delta t/T$ (the fraction of

the time period spent in the short axis direction) and asymptotically approaching a value of nM_S, where M_s is the saturation magnetization and where $n < 1$ depends on the magnetization rotation process. The MOKE measurements described below are obtained after saturating the sample along the long easy axis, turning off the magnetic field, and then measuring the component of magnetization along the short axis as a function of increasing and decreasing strain. After the strain measurements are completed, the magnetization signal along the short axis is measured in a large applied magnetic field of 0.35 T, well above the saturation field, allowing us to normalize our results to the saturation magnetization. Each run is normalized independently because, although the average domain structure of the entire sample remains the same from run to run, the "local" domain structure as measured by our beam spot can change due to pinning to local defects during saturation, and probe position change.

IV. MEASUREMENTS

In contrast to the coherent rotation observed in the 40 μm × 10 μm bars, experiments on these longer bars with aspect ratios of $\sim 10^3$ indicate a clear irreversibility. In Figure 4, we show the behavior of the short axis MOKE signal as a function of increasing and decreasing applied voltage (which is proportional to strain) on one sample, the sample measured at NIST, with an r.m.s. edge roughness of 2.3 nm. There is clear indication of irreversibility in the decreasing strain signal, showing that even after the strain has decreased to zero, a small fraction of the magnetization remains pinned along the short axis direction. Moreover, as the strain increases and the short axis magnetization signal saturates, the maximum magnetization signal lies below the expected value of $0.25M_S$, saturating at $0.225M_S$. The entire sample set shows qualitatively similar behavior, showing a sharp turn-on of the short axis magnetization, followed by an increase and an asymptotic approach to a maximum magnetization fraction at voltages well below the maximum applied voltage of 1.5 V. These behaviors (the threshold voltage, the asymptotic approach to saturation, and the dependence of the short axis magnetization on applied strain) provide supporting evidence for a simple coherent rotation model in which increasing strain above the threshold value has the effect of increasing the fraction of time that the magnetization is aligned along the short axis direction. However, the values of the threshold voltage with increasing and decreasing voltage amplitude, V_{ON} and V_{OFF}, respectively, the pinned magnetization ($(M/M_S)_{PIN}$) and the maximum magnetization ($(M/M_S)_{MAX}$) vary. In particular, $(M/M_S)_{MAX}$ remains below $0.25M_S$, ranging from $0.24M_S$ to $0.16M_S$ with increasing edge roughness.

We plot these quantities, together with the coercive field obtained from MOKE hysteresis loops as a function of edge roughness in Figure 5. The maximum value(s) of short axis magnetization, obtained at an applied r.f. voltage of 1.5 V, shows a monotonic decrease with increasing roughness, implying that increasing roughness results in a substantial fraction of the sample being pinned along the long axis direction, impervious to rotation via fast SAW generated

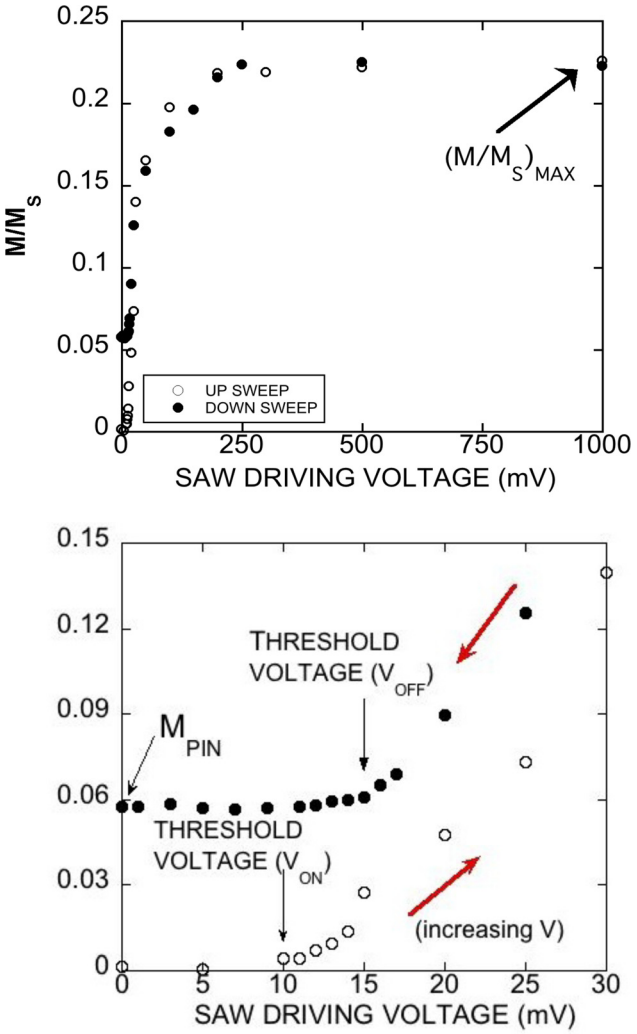

FIG. 4. MOKE signal for magnetization along the short axis direction as a function of SAW driving voltage for increasing and decreasing voltage on sample 2, the sample measured by PNR. (a) The entire voltage range and the maximum DC value of magnetization obtained by strain $(M/M_S)_{MAX}$. The expanded horizontal scale of (b) indicates the threshold voltages for increasing and decreasing voltage sweeps (V_{ON} and V_{OFF}) and the pinned magnetization (M_{PIN}).

magnetostriction. In contrast, the magnetization fraction that remains pinned along the short axis direction after the strain is reduced to zero, $(M/M_S)_{PIN}$, is fairly constant at about 0.06Ms. These results provide indirect evidence that the strain induced magnetization changes do result in multiple domains, along and perpendicular to the long axis in these very long bars. For the samples with the largest edge roughness, the fraction of domains that remain aligned along the long axis direction impervious to rotation is as high as 36% (obtained by taking the difference between the expected value of $(M/Ms)_{MAX} = 0.25$ and the actual measured value of $(M/Ms)_{MAX} = 0.16$) for the highest edge roughness. The fraction that remained pinned along the short axis direction when the strain is turned off is much smaller ($\sim$6% of the saturation magnetization) and shows no correlation with edge roughness.

The threshold voltage V_{ON}, ranging from 11–15 mV is related to the minimum strain e_o, required to initiate rotation of the magnetization into the short axis direction and is given

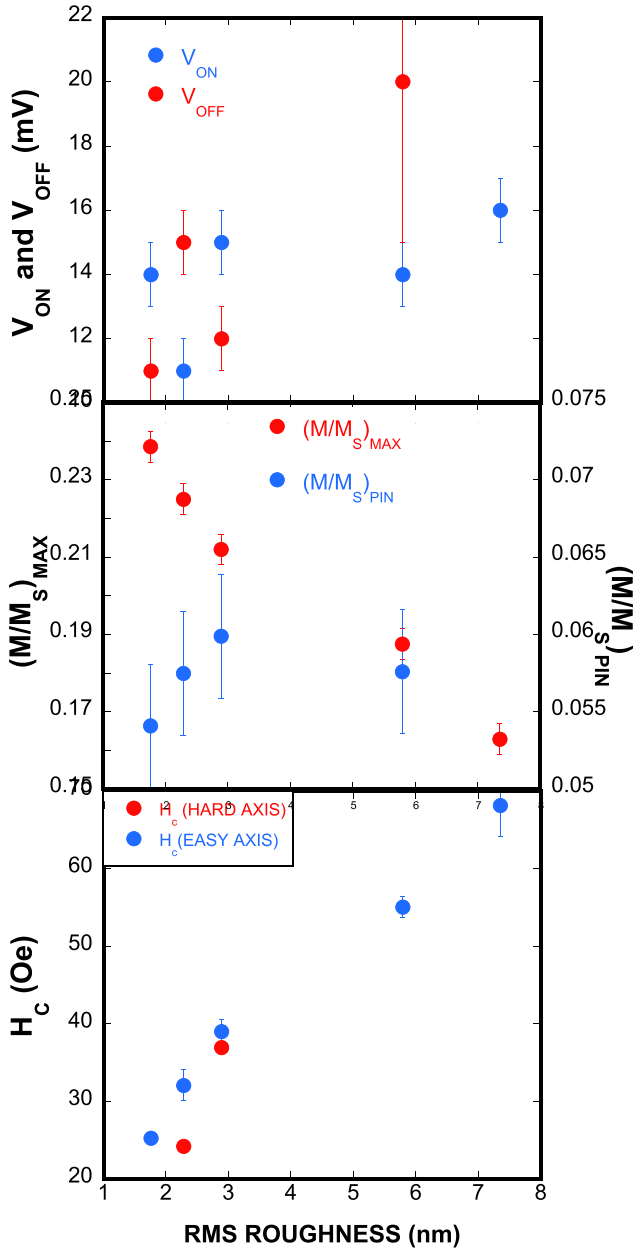

FIG. 5. Top: Threshold voltage for increasing (V_{ON}) and decreasing (V_{OFF}) voltages as a function of edge roughness. There does appear to be a slight increase of the average value with increasing roughness, but there is no dependence on roughness for the difference between the two. The turn on voltage corresponds to the minimum strain necessary to rotate the magnetization into the short axis direction. Middle: Maximum magnetization fraction $(M/M_S)_{MAX}$ (red) along the short axis direction that is strain driven and fraction of magnetization (blue) pinned along the short axis when strain is turned off, $(M/M_S)_{PIN}$, both as a function of edge roughness. Bottom: Coercive field along the long axis (blue) and short axis (red) as a function of edge roughness, showing a monotonic increase in the coercive field.

by $B_1|e_{33}| > K_s$. Because the strain amplitude of the SAW, e_{33}, and the magneto-elastic coefficient B_1 are highly dependent on the geometry of the IDT and the thickness of the film, respectively, the magnetization rotates into the short axis direction only when the product of the two exceeds K_s. Both threshold voltages, V_{on} and V_{off}, for increasing and decreasing voltage, respectively, are shown as a function of edge roughness. Ideally, for purely coherent rotation, the two should be identical, which is clearly not the case. However, the differences between them are small from which we can assume that most of the magnetization rotation seen is dominated by non-hysteretic processes. V_{ON} and V_{OFF}, and the difference between the two are independent of edge roughness, unlike the coercive fields, which show a monotonic increase with increasing roughness. This behavior of the coercive field is consistent with measurements on permalloy nanostructures,[17] which indicate that coercivity increases with increasing edge roughness, but, in general, experimental studies of the effects of edge roughness in ferromagnetic nanostructures are scarce. Micromagnetic simulations of the effects of periodic[18] edge roughness in Ni bars indicate that the coercive field decreases with roughness, whereas random edge roughness[19] is shown to increase the coercive field in FeNi bars. The former effect is ascribed to the nucleation sites provided by rough edges that enhance magnetization reversal, whereas the latter is attributed to the wide range of stable domain patterns that result from edge roughness. Because the threshold voltage V_{ON} corresponds to the minimum strain necessary to rotate the magnetization away from the long axis, one would expect its behavior to parallel that of the long axis coercive field and it is possible that these differing behaviors could imply that the driving mechanisms for domain unpinning and/or rotation are quite distinct for strain vs. magnetic field. Below, we offer an alternative explanation.

If we assume that the effects of dc strains are comparable to the effects of our 88 MHz SAW driven strain with a period of 11 ns, we can compare our data to experiments on dc strain driven magnetization rotation and/or domain formation. Strain driven magnetization reversal of a macroscopic Ni disc on a piezoelectric actuator indicate that the mechanisms for strain driven and field driven magnetization reversal are similar,[20] with short axis magnetization reversal dominated by coherent rotation and easy axis reversal showing domain formation close to the switching strain. In contrast, strain-driven magnetization reorientation in highly magnetostrictive microstructures of thin film FeGa (Ref. 21) proceeds solely via movement of domain walls. Simulations of magnetic thin films[22] indicate the mechanism for strain-driven switching is size dependent, with single domain coherent rotation for small lateral structures and domain formation for larger structures. Because the time period of the strain wave at 88 MHz is well above intrinsic time scales for magnetization reversals (which are ~100 ps) our assumption of equivalence between dc and fast strain may be true for coherent rotation mechanisms, but is unlikely to be so for domain wall motion. Domain wall velocities in Co wires peak at about 50 m/s,[23,24] although velocities as high as 500 m/s have been obtained in specialized geometries.[25] At these velocities, the time for domain walls to move across the 12 μm Co bar, 240 ns, is much longer than the period of the strain excitation, the SAW will not drive domain wall motion to any appreciable extent and the majority of the magnetization changes are due to the fraction of the bar that undergoes coherent rotation. We emphasize that this is not an issue of measurement—we measure the net total magnetization in the short axis direction—rather that strain waves at this frequency do not move domain walls. In contrast, the magnetic field (which is swept very slowly) results in both domain

wall motion and coherent rotation. Under this scenario, the monotonic decrease in $(M/M_S)_{MAX}$ with increasing edge roughness may be ascribed to the increasing importance of domain wall processes in samples with rough edges. Hence, the fast SAW waves drive a substantial fraction of the bars into the short axis direction via coherent rotation processes, and this fraction decreases with increasing edge roughness, as the fraction of domains impervious to fast magnetostriction increase.

Because MOKE measurements measure only a single component of magnetization, the aim of the PNR experiments was to isolate the magnetization component that rotates perpendicular to the original applied field when the SAW is turned on. All PNR measurements were made on the sample with an rms edge roughness of 2.3 nm. To maximize the sensitivity to the rotated magnetization, the magnetization of the sample was first aligned in a field of 0.1 T applied parallel to the long axis of the bars. For the PNR measurement, the sample was then oriented in near remanence with the short axis of the bars parallel to the small guide field of 1 mT such that the magnetic scattering appears only in the spin flip (SF) channel, as shown in Figure 1(a). The results of this SAW off PNR measurement, along with the fit using REFL1D,[26] are shown in Figure 6(a). In the absence of strain, the magnetization points predominantly along the long axis direction, perpendicular to the neutron spin, giving rise to a large SF signal. The non-spin flip (NSF) channel shows little to no difference in the intensity of spin-up and spin-down reflectivity. The spin asymmetry (SA),

$$SA = \frac{R^{++} - R^{--}}{R^{++} + R^{--}} \tag{3}$$

is a direct measure of the magnetization along the direction of spin polarization, i.e., along the short axis of the stripe. The spin asymmetry for the SAW off state (Figure 7(a)) is relatively flat, within error, indicating that the magnetization along the spin polarization direction perpendicular to the stripe edges is nearly zero, as expected.

PNR measurements taken with the SAW on (Figure 6(b)) indicate that the effect of the strain wave is, as expected, to rotate a fraction of the sample magnetization into the short axis direction. Qualitatively, this effect can be seen in the spin asymmetry shown in Figure 7(a). The increase in the magnitude of the spin asymmetry with the SAW on relative to SAW off (e.g., near Q = 0.03 and

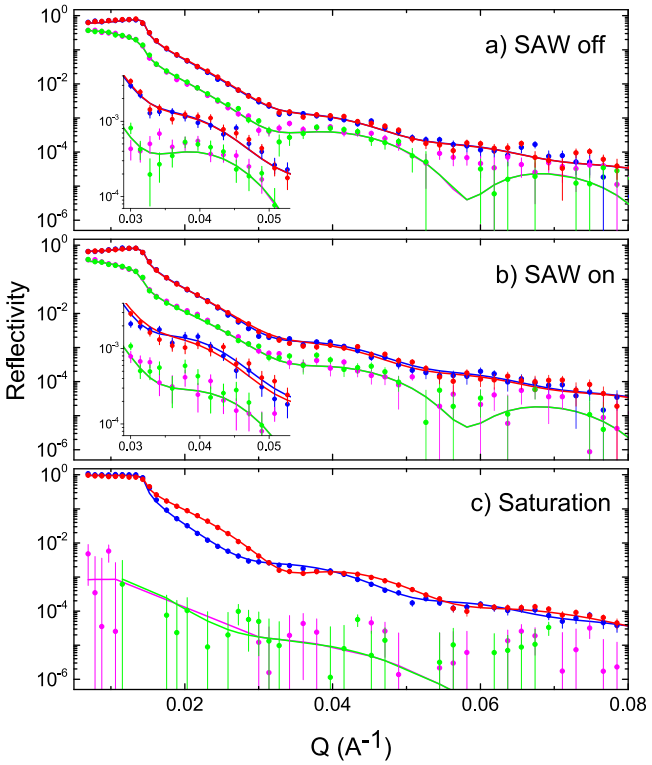

FIG. 6. Polarized neutron reflectivity data and corresponding fits made using REFL1D (solid lines) for all four cross sections, R^{++}(blue), R^{+-}(green), R^{-+} (pink) and R^{--}(red). (a) SAW off, with magnetization along the long stripe axis, perpendicular to the guide field (b) SAW on with magnetization components in both in-plane directions and (c) magnetization saturated along the short axis direction, parallel to the guide field. Insets in (a) and (b) highlight one of the Q regions in which the SAW off and SAW on reflectivities differ. The SAW driving voltage is 1.5 V.

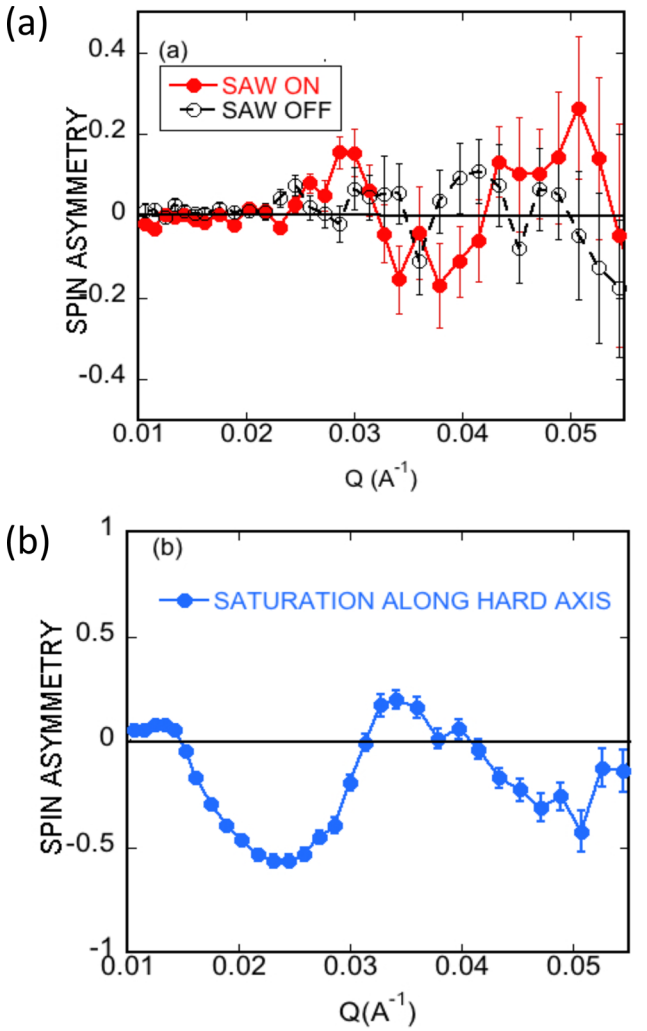

FIG. 7. The spin asymmetry, a measure of the magnetization component along the short axis of the rectangular Co bars. (a) With SAW off, the magnetization lies along the long axis of the bars. With the SAW on, the magnetization component along the short axis direction increases. (b) The maximum spin asymmetry for magnetization saturated along the short axis. Note the different vertical scales in (a) and (b). The SAW driving voltage is 1.5 V.

$0.04\,\text{Å}^{-1}$) is indicative of an increase in the magnetization along the short axis direction. For comparison, the maximum spin asymmetry is obtained for the case of a 0.1 T field applied along the short axis (Figure 7(b)), corresponding to alignment of the magnetization parallel to the applied field. Features (i.e., dips and peaks) in the spin asymmetry for the short-axis saturation and SAW on cases appear at similar values of Q (approximately $0.022\,\text{Å}^{-1}$, $0.033\,\text{Å}^{-1}$, and $0.051\,\text{Å}^{-1}$), though the sign is *opposite* and the magnitudes are smaller. This behavior suggests that the fraction of the magnetization that rotates is reduced relative to the saturation magnetization, and the magnetization rotates in a direction *opposite* that of the applied field, as discussed below.

A similar trend is seen in the spin flip data (Figure 8), which is also consistent with rotation of the remanent magnetization away from the long axis when the SAW is turned on. In the SAW off state, the large Co magnetization perpendicular to the guide field (along the stripe edge) gives rise to pronounced spin flip scattering (Figure 6(a)) at the expense of non-spin flip scattering. When the SAW is turned on, the spin flip scattering decreases (and the total non-spin flip scattering correspondingly increases) just above and well below the critical angle near $Q = 0.015\,\text{Å}^{-1}$ in the region nominally corresponding to total internal reflection. This reduction indicates that the projection of the net magnetization parallel to the stripe edge has decreased. The spin flip intensity (Figure 8) also shows a change in shape well above the critical angle with a slight decrease in intensity of the SAW on relative to SAW off near $Q = 0.04\,\text{Å}^{-1}$. In a saturating 0.1 T field applied along the short axis (Figure 6(c)), the spin flip scattering below the critical angle is absent and the non spin flip reflectivity equals one (i.e., total internal reflection), as expected, since the magnetization is aligned parallel to the applied field.

Quantitative fitting of the PNR data is complicated by the mixture of coherent and incoherent sums that accounts for the incomplete coverage of the Co on the $LiNbO_3$ substrate and for the possible presence of magnetic domains of varying size. Specifically, we assume that the scattering from the Co-covered regions adds incoherently to that from the bare substrate. Using the REFL1D software,[26] we performed simultaneous fits of the SAW off, SAW on, and short axis saturation data (solid lines in Figure 6) and determined the ratio of the covered to uncovered fraction of the sample to be 1:1.65. This ratio corresponds to 38% Co coverage (1/2.65), which is consistent with AFM measurements for this sample. Since models with a single, uniform Co layer were unable to reproduce the beating pattern in the data, the nominal Co layer was divided into four sub-layers of variable thickness to allow for depth-dependent variations in the nuclear composition and magnetic structure. The nuclear scattering length profile for the Co-covered region, determined from simultaneous fits of all three data sets (Figure 6), with the structural parameters constrained to match is shown in Figure 9(a)). The Co layer is capped with a rough 5 nm layer with a reduced scattering length density that may originate from the formation of a porous oxide, though the scattering length density is somewhat smaller than that of bulk CoO. The remainder of the Co layer is structurally uniform, and the interface between the Co and $LiNbO_3$ has a full-width of approximately 0.7 nm.

The best fits to the data in all three conditions (Figure 6) reveal a complex, depth-dependent spin structure that does

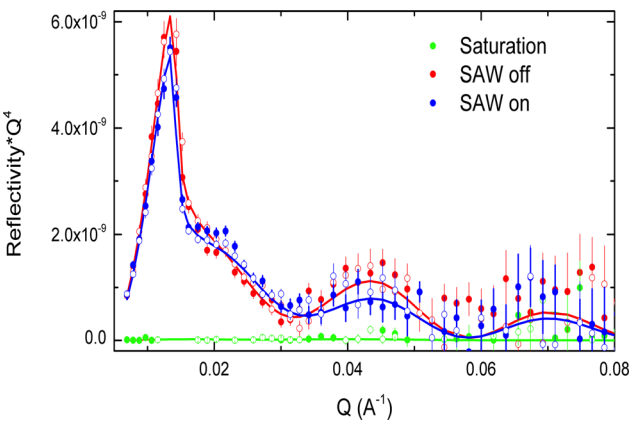

FIG. 8. Spin flip reflectivity (multiplied by Q^4), a measure of the magnetization along the long axis of the Co bars. The open and closed symbols are R^{--} and R^{+-}, respectively. The solid lines are the fits to the data (see text) After saturation along the long axis (see text) and with the SAW off, the spin flip reflectivity is sizable, decreasing when the SAW is turned on because some fraction of the magnetization rotates into the short axis direction. Magnetic saturation along the short axis direction substantially reduces the spin flip reflectivity. The SAW driving voltage is 1.5 V.

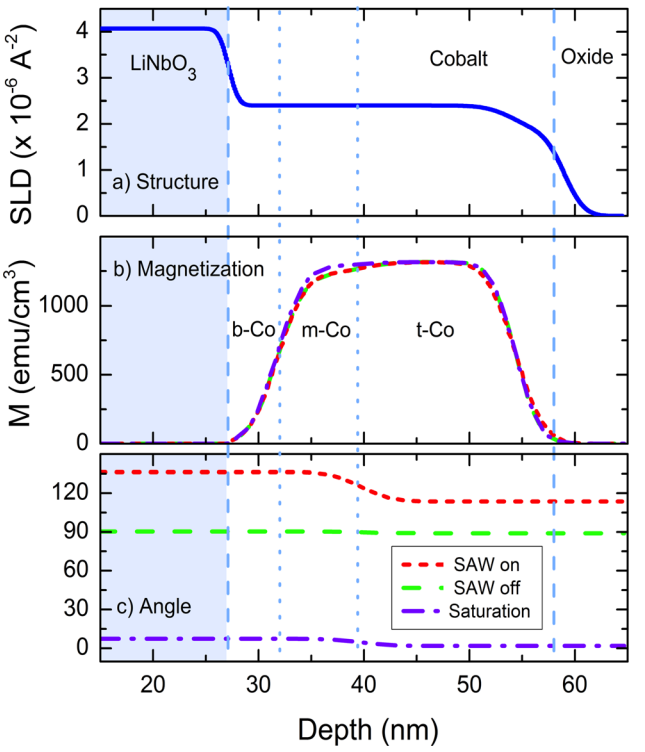

FIG. 9. Depth dependence of (a) the nonmagnetic scattering length density (SLD), (b) the total magnetization, and (c) the angle of magnetization for SAW off, SAW on, and magnetic saturation as obtained from fits to the PNR data. The fits are constrained to the same SLD for all three. Note that the magnetization of the Co layer varies across the thickness, but that the net magnetization is nearly constant for SAW off, SAW on, and magnetic saturation as expected. The angle of magnetization changes considerably with SAW on, and the Co layers closer to the $LiNbO_3$ rotate further than those farther away.

not track the nuclear structure of the Co layer, as shown in Figure 9. As an example, the short axis saturation data (Figure 6(c)) are best described by a model that includes a complete suppression of the in-plane magnetization in the bottom section (thickness of 4.60 nm) of the Co layer adjacent to the substrate. The origin of this magnetically inactive region is unknown though it is possible that the Co structure or strain leads to local regions with a higher anisotropy or with perpendicular anisotropy that do not saturate in a 0.1 T field. The magnetization in the remaining portion of the Co layer is not uniform but rather obtains a maximum value of 1280 emu/cm^3 in the center region (7.95 nm thick) and a slightly larger value of 1310 emu/cm^3 in the top 14.6 nm region adjacent to the CoO cap. Note that the overall magnetization of the entire Co layer is reduced relative to the bulk Co magnetization of 1420 emu/cm^3. In addition, the Co magnetization is not completely perpendicular to the stripe edge but is canted at an angle of 7.4° relative to the applied field in the center section and canted at a small angle of 1.8° at the top (Figure 9(c)). The slight tipping of the center and top magnetization is required to account for the residual spin flip scattering above the critical angle (Figure 6(c)) and indicates that the 0.1 T field is not sufficient to align fully the magnetization along the short axis of the stripes.

The spin structure for the SAW off remanent state (Figures 9(b) and 9(c)) is similar to that of the short axis saturation state. As expected, the magnetization is aligned nearly parallel to the stripe edge since the sample was first magnetized in a 0.1 T field applied parallel to the long axis of the stripe. Specifically, the in-plane magnetization in the bottom 4.6 nm of the Co layer is again equal to zero. The center section of the Co layer, which is 7.95 nm thick, has a magnetization of 1220 emu/cm^3 that is aligned at an angle of 90.3° relative to the guide field (note that the stripe edge is at 90° by this definition). The magnetization in the top section of the Co layer (14.6 nm thick, just below the oxide cap) has a slightly higher magnetization of 1310 emu/cm^3 that is canted at an angle of 89.1°. While the fits are not particularly sensitive to the precise thickness of the regions with differing vector magnetizations, the data cannot be fit with a single Co layer with uniform magnetization. Overall, the Co magnetization in the SAW off state is aligned nearly parallel to the stripe edge with a magnetization gradient through the film depth that is more pronounced than the gradient obtained in saturation. Since the magnetization at each depth represents the average across the sample plane assuming coherent addition of the scattering, it is possible that the reduced net magnetization in the central depth originates from the formation of small (<100 μm) in-plane (or out-of-plane) magnetic domains only in the portion of the stripes closest to the substrate.

Quantitative analysis of the SAW on data is more challenging as the time-averaged reflectivity includes contributions from the moments in approximately half of the stripes that are aligned parallel to the stripe edges at all times (Figure 3) and from the moments in alternate stripes that potentially form in-plane domains when they rotate away from the edges. While the complete structure and magnetic configuration of the sample cannot be obtained by a unique inverse transform of the data (as is the case in almost all scattering problems), we can apply realistic constraints to a model based upon the expected magnetic configuration (Figure 3) in which the magnetization in alternate Co stripes rotates. It is assumed that the magnetization in every other stripe is aligned nearly parallel to the edges at any given time, with values of the depth-dependent magnetization and canting angles that match those obtained from fitting the SAW off PNR data in Figure 6(a). The depth-dependent magnetization and canting angle in the remaining half of the stripes are allowed to vary. The scattering from these two regions are then added incoherently, since the transverse neutron beam coherence has been demonstrated to be well below 5 μm on this instrument.[27]

It is notable that the fit reproduces unique features in the SAW on reflectivity near the critical angle and in other Q regions (inset of Figure 6(a)) that differ from those in the SAW off reflectivity. The best fit (solid line in Figure 6(b)) reveals that rotating stripes have a magnetization M_t in the top region of the Co layer ($t_t = 14.6$ nm thick) of 1310 emu/cm^3 (consistent with the SAW off value) at an angle of 113.6°, which is significantly rotated away from the stripe edge at 90°. The middle section of the Co layer ($t_m = 7.95$ nm thick) has a magnetization M_m of 1230 emu/cm^3 (again consistent the corresponding SAW off value) at an even larger angle of 136.3° (Figures 9(b) and 9(c)). In the SAW on state, the moments in the top and middle regions of the Co layer rotate relative to their SAW off positions by $\theta_t = 46.0°$ and $\theta_m = 24.5°$, respectively. The canting angles obtained from the fits represent the average over time (i.e., time spent above and below the threshold strain) and the average across the sample plane, and locally the moments may rotate by as much as ±90° depending upon their proximity to pinning sites. It is notable, however, that the magnitude of the Co magnetization obtained from the fits matches that obtained for the SAW off state (Figure 9(b)), indicating that the Co magnetization rotates coherently and local domain formation during rotation is quite limited. Based upon the fit, the fraction of the SAW off magnetization that rotates is approximately 26%, as determined from the weighted ratio of the rotated magnetization relative to the short axis saturation magnetization

$$\frac{t_m M_m \,\mathrm{Sin}(\theta_m) + t_t M_t \,\mathrm{Sin}(\theta_t)}{t_m M_{SAT-m} + t_t M_{SAT-t}}, \tag{4}$$

where $M_{\mathrm{SAT\text{-}m}} = 1280$ emu/cm^3 and $M_{\mathrm{SAT\text{-}t}} = 1310$ emu/cm^3 are the short axis saturation magnetizations of the middle and top Co layers, respectively. The SAW on (and SAW off) value of M_m (1230 emu/cm^3) compared to the saturation value of $M_{\mathrm{SAT\text{-}m}}$ (1280 emu/cm^3) may originate from in-plane domain formation. The perpendicular magnetization component thus corresponds to 1/4th of the short axis saturation magnetization, in agreement with the MOKE results.

While the fit above is not unique as the exact nature and size of in-plane domains is unknown, alternate approaches to fitting the data consistently indicate that 22%–28% of the magnetization rotates away from the stripe edge when the SAW is turned on. Surprisingly, the magnetization preferentially rotates antiparallel (rather than parallel) to the small

applied field in the SAW on state. We assume that defects, strain, or other structural non-uniformities somehow break the two-fold symmetry of the stripe geometry. In addition, the degree of rotation of the magnetization has a clear dependence upon depth in the Co layer, with more pronounced rotation nearest the Co/substrate interface. It is significant, however, that the magnitude of the magnetization throughout the depth of the Co layer (Figure 9(b)) is preserved in the SAW on state relative to SAW off. The PNR data thus fully support a model involving coherent rotation of the magnetization as the formation of small, local domains during rotation would give rise to a reduction in the magnitude of the magnetization since it corresponds to the average across the sample plane.

V. CONCLUSIONS

We have successfully used high frequency (88 MHz) strain waves in piezoelectric $LiNbO_3$ to rotate the magnetization of long Co bars with aspect ratios $>10^3$ into the short axis direction. With increasing edge roughness, the fraction of magnetization rotates into the short axis direction decreases. We attribute this to the short time period of the high frequency SAW wave, resulting in domain walls that are unresponsive to the rapidly alternating tensile and compressive strains. The domains are effectively frozen into place because the strain that acts as the driver for domain wall motion oscillates over time scales much shorter than those for domain wall motion. SAW waves at this high frequency can rotate magnetization but cannot move domain walls, setting a limit for the temporal response of strain driven magnetization changes.

Both MOKE and polarized neutron reflectivity measurements confirm this behavior, showing an increase in magnetization along the short axis direction when the SAW is turned on. In addition PNR measurements indicate that the magnetization along the long axis decreases when the SAW is on, but this decrease is clearly not the result of formation of small, in-plane domains. The overall magnitude of the rotated magnetization obtained from quantitative fits, using a model in which alternating bars rotate into the short axis direction, closely matches that obtained from MOKE.

The agreement between the MOKE and PNR measurements is important because they are sensitive to different aspects of the magnetization. MOKE measurements are qualitative, probe only one component of magnetization and are also susceptible to changes in the refractive index of $LiNbO_3$, a highly electro-optically active material. PNR measurements enable a measurement of both magnetization components simultaneously, are quantitative, and are blind to the effects of changing refractive indices. Combined with MOKE, the PNR reveals that coherent rotation, rather than domain formation, is the dominant mechanism for fast strain driven magnetization switching even when the aspect ratio of the ferromagnetic bars is extremely large; furthermore, the effect is non-uniform across the thickness of even these very thin magnetic elements, suggesting that total control of the strain profile in devices will be critical to their performance.

ACKNOWLEDGMENTS

This work was supported by the National Science Foundation under grant NSF MRSEC-0820521.

[1]A. Kirilyuk, A. V. Kimel, and T. Rasing, Rev. Mod. Phys. **82**, 2731 (2010).
[2]J. Stöhr and H. C. Siegmann, *Magnetism: From Fundamentals to Nanoscale Dynamics*, Series in Solid-State Sciences (Springer, 2006), Chap. 15.
[3]J.-Y. Bigot, M. Vomir, and E. Beaurepaire, Nat. Phys. **5**, 515 (2009).
[4]C. H. Back, D. Weller, J. Heidmann, D. Mauri, D. Guarisco, E. L. Garwin, and H. C. Siegmann, Phys. Rev. Lett. **81**, 3251 (1998).
[5]T. H. E. Lahtinen, J. O. Tuomi, and S. van Dijken, Adv. Mater. **23**, 3187 (2011).
[6]R. V. Chopdekar, V. K. Malik, A. Fraile Rodrıguez, L. Le Guyader, Y. Takamura, A. Scholl, D. Stender, C. W. Schneider, C. Bernhard, F. Nolting, and L. J. Heyderman, Phys. Rev. B **86**, 014408 (2012).
[7]C. Krischer, I. Feng, J. B. Block, and M. Levy, Appl. Phys. Lett. **29**, 76 (1976).
[8]I. Feng, M. Tachiki, C. Krischer, and M. Levy, J. Appl. Phys. **53**, 177 (1982).
[9]M. Levy and H. Yoshida, J. Magn. Magn. Mater. **35**, 139 (1983).
[10]D. Walikainen, R. F. Wiegert, and M. Levy, J. Appl. Phys. **63**, 3927 (1988).
[11]M. Weiler, L. Dreher, C. Heeg, H. Huebl, R. Gross, M. S. Brandt, and S. T. B. Goennenwein, Phys. Rev. Lett. **106**, 117601 (2011).
[12]L. Dreher, M. Weiler, M. Pernpeintner, H. Huebl, R. Gross, M. S. Brandt, and S. T. B. Goennenwein, Phys. Rev. B **86**, 134415 (2012).
[13]J.-W. Kim, M. Vomir, and J.-Y. Bigot, Phys. Rev. Lett. **109**, 166601 (2012).
[14]S. Davis, A. Baruth, and S. Adenwalla, Appl. Phys. Lett. **97**, 232507 (2010).
[15]M. Luenneman, U. Hartwig, G. Panotopopoulos, and K. Buse, Appl. Phys. B **76**, 403 (2003).
[16]Strictly speaking, all MOKE measurements are obtained at 50 kHz, the frequency of the PEM. However, the much higher SAW resonance frequency of 88 MHz results in averaging over $>10^3$ cycles.
[17]M. T. Bryan, D. Atkinson, and R. R. P. Cowburn, Appl. Phys. Lett. **85**, 3510 (2004).
[18]J. Gadbois and J.-G. Zhu, IEEE Trans. Magn. **31**, 3802 (1995).
[19]J. G. Deak and R. H. Koch, J. Magn. Magn. Mater. **213**, 25 (2000).
[20]A. Brandlmaier, M. Brasse, S. GeprÅNags, M. Weiler, R. Gross, and S. T. B. Goennenwein, Eur. Phys. J. B **85**, 124 (2012).
[21]D. E. Parkes, S. A. Cavill, A. T. Hindmarch, P. Wadley, F. McGee, C. R. Staddon, K. W. Edmonds, R. P. Campion, B. L. Gallagher, and A. W. Rushforth, Appl. Phys. Lett. **101**, 072402 (2012).
[22]J.-M. Hu, G. Sheng, J. X. Zhang, C. W. Nan, and L. Q. Chen, Appl. Phys. Lett. **98**, 112505 (2011).
[23]T. Koyama, D. Chiba, K. Ueda, H. Tanigawa, S. Fukami, T. Suzuki, N. Ohshima, N. Ishiwata, Y. Nakatani, and T. Ono, Appl. Phys. Lett. **98**, 192509 (2011).
[24]K. Yamada, J.-P. Jamet, Y. Nakatani, A. Mougin, A. Thiaville, T. Ono, and J. Ferre′, Appl. Phys. Express **4**, 113001 (2011).
[25]P. J. Metaxas, J. Sampaio, A. Chanthbouala, R. Matsumoto, A. Anane, A. Fert, K. A. Zvezdin, K. Yakushiji, H. Kubota, A. Fukushima, S. Yuasa, K. Nishimura, Y. Nagamine, H. Maehara, K. Tsunekawa, V. Cros, and J. Grollier, Nat. Sci. Rep. **3**, 1829 (2013).
[26]B. J. Kirby, P. A. Kienzle, B. B. Maranville, N. F. Berk, J. Krycka, F. Heinrich, and C. F. Majkrzak, Curr. Opin. Colloid Interface Sci. **17**, 44 (2012).
[27]C. F. Majkrzak, C. Metting, B. Maranville, J. A. Dura, S. Satija, T. Udovic, and N. F. Berk, Phys. Rev. A **89**, 033851 (2014).
[28]G. P. Felcher, R. O. Hilleke, R. K. Crawford, J. Haumann, R. Kleb, and G. Ostrowski, Rev. Sci. Instrum. **58**, 609 (1987).
[29]M. R. Fitzsimmons and C. F. Majkrzak, "Application of polarized neutron reflectometry to studies of artificially structured magnetic materials," in *Modern Techniques for Characterizing Magnetic Materials*, edited by Y. Zhu (Springer, 2005).
[30]S. Polisetty, J. Scheffler, S. Sahoo, Y. Wang, T. Mukherjee, X. He, and C. Binek, Rev. Sci. Instrum. **79**, 055107 (2008).